Journal of Astronomical Telescopes, Instruments, and Systems

AstronomicalTelescopes.SPIEDigitalLibrary.org

In-orbit robotic assembly mission design and planning to construct a large space telescope

Yuchen She
Shuang Li
Yufei Liu
Menglong Cao

SPIE.

Yuchen She, Shuang Li, Yufei Liu, Menglong Cao, "In-orbit robotic assembly mission design and planning to construct a large space telescope," *J. Astron. Telesc. Instrum. Syst.* **6**(1), 017002 (2020), doi: 10.1117/1.JATIS.6.1.017002

In-orbit robotic assembly mission design and planning to construct a large space telescope

Yuchen She,[a] Shuang Li,[a,*] Yufei Liu,[b] and Menglong Cao[c]

[a]Nanjing University of Aeronautics and Astronautics, College of Astronautics, Nanjing, China
[b]China Academy of Space Technology, Qian Xuesen Laboratory of Space Technology, Beijing, China
[c]Qingdao University of Science and Technology, College of Automation and Electronic Engineering, Qingdao, China

Abstract. We investigate the conceptual design and in-orbit assembly mission planning problem of a large space telescope (LST). The segmented mirror design has been proposed, and the robotic assembly concept considering the manipulator work space coverage is developed. To reduce the in-orbit assembly period and protect the fragile mirror structure, the assembly paths of the robots are optimized by several new algorithms. First, a mapping between the assembly path and the assembled piece number is established to rapidly generate the candidate solution to the optimization problem. Second, the two-level hybrid optimization framework that combines the ant-colony-inspired algorithm and the genetic algorithm is proposed. The hybrid optimization method is designed to be able to converge rapidly to a solution that is close to the global optimal point. The proposed models and algorithms are verified by simulation, and the results show that the methods developed can dramatically increase the in-orbit assembly mission efficiency of an LST. © *2020 Society of Photo-Optical Instrumentation Engineers (SPIE)* [DOI: 10.1117/1.JATIS.6.1.017002]

Keywords: large space telescope; robotic assembly; segmented mirror; assembly mission planning.

Paper 19035 received Apr. 11, 2019; accepted for publication Jan. 2, 2020; published online Jan. 21, 2020.

1 Introduction

The construction of a large space telescope (LST) is significantly important for scientific research and engineering applications.[1,2] As the size of the telescope reflector continues to increase, the future LST will be launched in pieces into space and will be assembled in orbit by robotic manipulators.[3,4] Since the LST often involves a huge number of modules with various functionalities, the in-orbit assembly process is a complex operation. Therefore, the LST in-orbit assembly mission planning is key to the success of the mission, and many works have been reported in this research area.

Regarding the LST design aspect, various conceptual designs of the LST such as the large solar space telescope concept have been proposed.[5] Another concept of large aperture space telescopes, which was designed to be launched by the Ares V launch vehicle, was proposed by Lille et al.[6] Pan and Xu[7] proposed the disturbed situational observer concept, which has made an important contribution in building the new-generation LST. In addition, since the LST is often equipped with a large flexible reflector, the dynamical analysis and vibration control of flexible space structures, which ensures the success of the mission, is also a major research topic. Mohan and Miller[8] proposed the new dynamical model to properly describe the motion of large space systems during the space assembly process. Shi et al.[9] proposed a robust controller of a large space servicing platform with flexible appendages, which ensures the stability of the large space structure during the robotic assembly operation. A similar approach was proposed by Bandyopadhyay and Chung[10] to realize the attitude control of a large spacecraft with high

*Address all correspondence to Shuang Li, E-mail: lishuang@nuaa.edu.cn

flexibility. Gasbarri et al.[11] developed the state-dependent Riccati equation-based controller to realize the vibration suppression control of large space structure with parameter uncertainty. Meanwhile, the slew path planning and scheduling problem of the LST have also been deeply investigated.[12,13]

Regarding the in-orbit assembly mission planning aspect, two major categories of the orbit assembly concept can be recognized: the human-involved assembly approach[14] and the autonomous in-orbit assembly approach.[15] Optimization algorithms have been proposed on both concepts to increase the efficiency of space assembly operation. The human-involved assembly concept is the classic research topic and has already made important contributions to real space missions such as the international space station[16] and the early concept of the James Webb Space Telescope. More recent research has focused on the autonomous assembly technology, which can be further classified into two subcategories: assembly based on the servicing platform and assembly by formation flying and docking maneuvering. The first approach is dedicated to assembling the modules using the space manipulators, and the mission planning of such scenarios is focused on assembly path designing and scheduling. In most cases, the artificial potential method is adopted with the symmetrical path constraint to generate the assembly path of the manipulator.[4] The author proposed a hybrid optimization algorithm to realize the assembly path planning, considering the topological constraint and the minimum attitude disturbance criterion.[17] In addition, many works have been conducted in the space manipulator control area to increase the assembly accuracy and reduce the system vibration.[18] The second approach is based on the spacecraft autonomous rendezvous (RDV) and docking technology. Every module is considered a small spacecraft with limited orbit and attitude control ability, and the assembly is realized by the formation flying and docking maneuvers. This concept has some advantages, such as high assembly accuracy, short assembly period, and high redundancy. Therefore, the RDV and docking assembly concept has also been deeply investigated to realize the LST assembly missions.[19] Another advantage of such technology is that the reconfiguration control of the large space system can be conducted by the autonomous RDV and docking principle, as illustrated by Underwood et al.[20] Many intelligent path planning and scheduling methods have been presented under this mission concept. Badawy and McInnes[21] proposed the superquadric potential field method for rapid autonomous assembly path planning. Similar approaches have also been presented to realize the efficient autonomous assembly,[22,23] and Chen et al.[24] addressed the collision avoidance control of the actuator clusters during the assembly process in considering the flexibility of the structure. However, the RDV and docking assembly principle also has certain drawbacks, including high risk of collision, high requirement for guidance, navigation and control systems, and large fuel consumption. To address this issue, this paper is focused on the first in-orbit assembly concept, which is based on the operation of space manipulators.

By analyzing the previous works, it can be seen that the current research has mainly focused on the feasibility analysis and the mission planning algorithm with a single robot, while the mission planning and scheduling of multirobot assembly operation has not been widely analyzed yet. During the real space telescope assembly mission, since the number of modules is large, multiple manipulators have to work together to accomplish the assembly operation. With the increasing number of manipulators, the task assignment, mission planning, and scheduling problems become more and more complex. Moreover, since the telescope mirror reflector is usually fragile, more constraints must be considered such as the minimum distance between robots and the no-overlap of tasks assigned to different robots. Therefore, the modified optimization problem becomes much more complex, and it can no longer be properly solved by the classic optimizers. To address this issue, the multirobot mission assignment, planning, and scheduling problem is investigated in this paper. First, to realize the in-orbit assembly of the large telescope mirror, the manipulator has to move along the parabolic mirror surface to carry the piece to the right position. The motion trajectory of the manipulator during the assembly process is characterized as the assembly path and is optimized in this paper. In addition, the work space coverage of the manipulator is also taken into consideration during the assembly path planning problem. The pieces within the work space of the manipulator are considered to be assembled and eliminated from the working list, which is more realistic and can reduce the calculation cost. Second, based on the multirobot assembly scenario, the safety distance constraint is considered in the mission-scheduling process,[25] and the time-delay factor is added into the algorithm to

obtain the maximum relative distance between robots. Third, a mathematical mapping is established to rapidly generate the assembly path with manipulator work space coverage, which serves as the candidate solution for the optimization problem. The genetic algorithm (GA)-based hybrid optimization algorithm is developed to properly solve the path planning and scheduling problem. The rest of the paper is organized as follows: Sec. 2 demonstrates the mission scenario and system design. Section 3 addresses the manipulator work space coverage and the delay factor, and the optimization algorithm is properly developed. The simulation results and analysis are shown in Sec. 4, before the conclusion is given in Sec. 5.

2 Mission Scenario and System Design

This paper considers the in-orbit assembly process of an LST's mirror reflector. To simplify the mathematical analysis of the problem, a specific mission scenario has been established and considered throughout this paper. The mission objective is to construct a 60-m parabolic space telescope mirror via the robotic assembly approach, as shown in Fig. 1. It should be clarified that the paper is only focused on the construction of the mirror reflector system using multiple manipulators, and the deployment of the satellite base is not considered. To simplify the calculation, the analysis of the problem is set to be in the mirror reflector local coordinate system $O_a - X_a Y_a Z_a$. It is assumed that the LST mirror is launched in modules and is assembled by multiple robots in space. The robot considered in this paper consists of a base and a manipulator and the moving trajectory of the base is the assembly path, which should be optimized. From Fig. 1, it can be noticed that the starting points of all of the assembly paths are set to be the central point of the mirror reflector, so the initial condition of the optimization problem is fixed.

To assemble the large telescope illustrated in Fig. 1, the segmented mirror design has been adopted and the reflector surface is set to be composed of 274 hexagonal pieces and six working regions. Each region is handled by one of the robots, and the assembly path is planned for each robot system. The two-dimensional (2-D) mission scenario is shown in Fig. 2, where the working regions are assigned to the robots R1 to R6, respectively. Therefore, the positions of all pieces are fixed in the $O_a - X_a Y_a Z_a$ throughout the mission, and they are noted as

$$\mathbf{P} = [\mathbf{v}_1 \quad \mathbf{v}_2 \quad \dots \quad \mathbf{v}_n], \tag{1}$$

$$\mathbf{v}_i = [x_i, y_i, z_i], \quad i = 1,2,\dots,274. \tag{2}$$

From Fig. 2, it can also be noticed that the working regions R3 and R5 are generated by rotating R1 and that R4 and R6 are generated by rotating R2, respectively. The number and

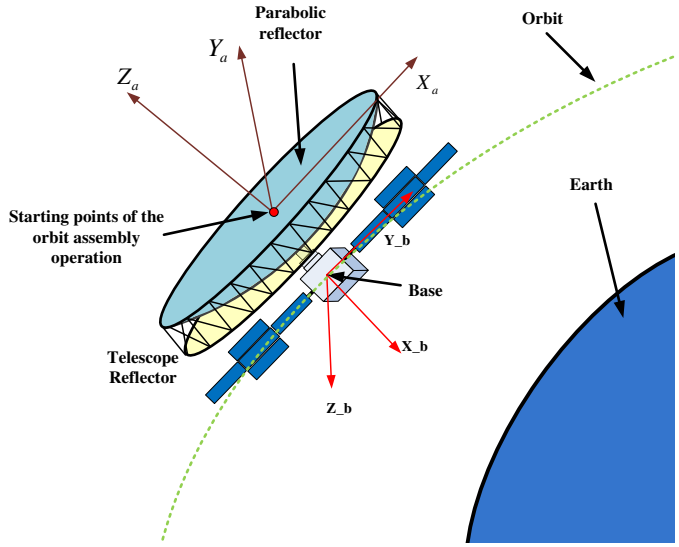

Fig. 1 Illustration of the mission scenario.

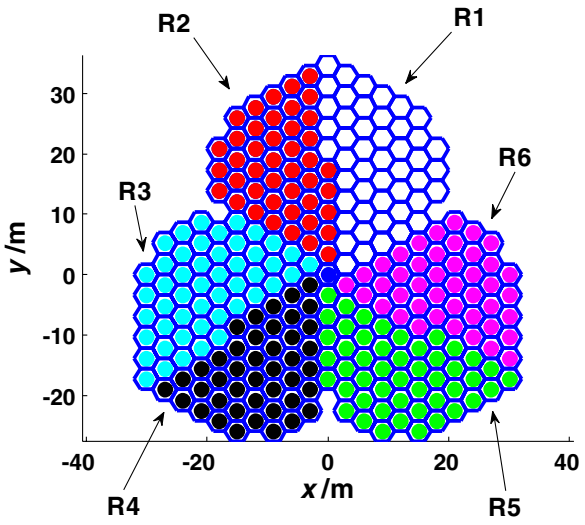

Fig. 2 Demonstration of task assignment for the six robots.

positions of the piece with R1 and R2 are predefined and fixed. Therefore, Eq. (1) is rewritten as

$$\begin{cases} \mathbf{P}_{R1} = [\mathbf{v}_1 \quad \mathbf{v}_2 \quad \dots \quad \mathbf{v}_{nR1}] \\ \mathbf{P}_{R2} = [\mathbf{v}_1 \quad \mathbf{v}_2 \quad \dots \quad \mathbf{v}_{nR2}] \end{cases}, \tag{3}$$

$$\begin{cases} \mathbf{P}_{R3} = \mathbf{q}_1 \otimes \mathbf{P}_{R1} \\ \mathbf{P}_{R5} = \mathbf{q}_2 \otimes \mathbf{P}_{R1} \\ \mathbf{P}_{R2} = \mathbf{q}_1 \otimes \mathbf{P}_{R2} \\ \mathbf{P}_{R6} = \mathbf{q}_2 \otimes \mathbf{P}_{R2} \end{cases}, \tag{4}$$

where $\mathbf{q}_1$ and $\mathbf{q}_2$ are the two quaternion vectors, which are given as

$$\begin{cases} \mathbf{q}_1 = \left[\cos\left(\frac{\pi}{6}\right), [0,0,1] \cdot \sin\left(\frac{\pi}{6}\right)\right]^T \\ \mathbf{q}_2 = \left[\cos\left(\frac{\pi}{3}\right), [0,0,1] \cdot \sin\left(\frac{\pi}{3}\right)\right]^T \end{cases}. \tag{5}$$

In Eq. (3), $nR1$ and $nR2$ are fixed to be 49 and 44, respectively. Thus, the assembly path generation is done within a subspace of $\mathbf{P}$ with smaller node number, which can dramatically reduce the calculation cost. Figure 3 demonstrates the relation between the three-dimensional (3-D) parabolic surface and its 2-D projection. The geometrical form of the surface is defined by the parabolic function:

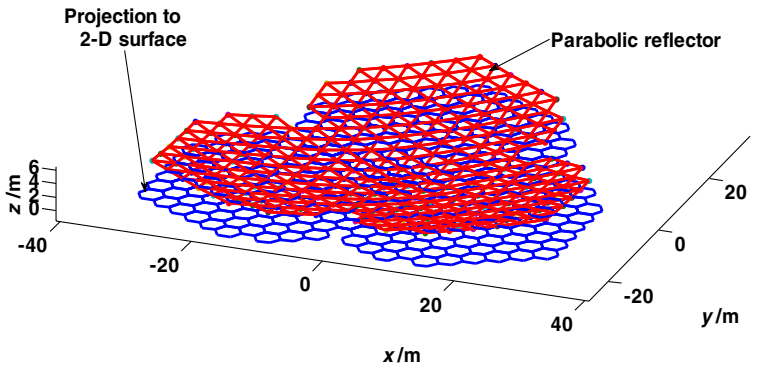

Fig. 3 A 3-D illustration of the telescope mirror reflector and the 2-D projection.

$$z(i) = a \cdot \left[\sqrt{x(i) + y(i)}\right]^{\gamma}, \tag{6}$$

where a and γ are the positive constant coefficients and the mission planning process is dedicated to minimize the length of the assembly path.

To create the optimization model, the connection matrix and the existence matrix are also defined and noted as $\mathbf{\Theta}$ and $\mathbf{E}(t)$, respectively. The detailed definition of these two matrices can be found in Ref. 17, so they will not be addressed in detail in this paper. At first, only the symmetrical assembly path criterion is considered, which means that the assembly path of R3 to R6 can be generated by rotating the path of R1 and R2 using the quaternions defined in Eq. (5). Therefore, the classic assembly problem is formulated as

$$\min_{\mathbf{N},\mathbf{M}}(a_1 \cdot L_l + a_2 \cdot L_r) \quad st. \begin{cases} \mathbf{N} = [N_1 \quad N_2 \quad \cdots \quad N_{44}] \\ \mathbf{M} = [M_1 \quad M_2 \quad \cdots \quad M_{49}] \\ N_i \neq N_j,\ M_i \neq M_j,\ \forall\ i \neq j \\ N_i = 1,2,3,\ldots, N_i \in [1,2,3,\ldots..,44] \\ M_i = 1,2,3,\ldots, M_i \in [1,2,3,\ldots..,49] \\ \mathbf{E}_i(t_f) = 1,\ \forall\ i = 1,2,3,\ldots,93 \end{cases}, \tag{7}$$

where $\mathbf{N}$ and $\mathbf{M}$ denote the assembly sequence of the left and right paths, respectively. The fourth line of Eq. (7) indicates that the piece that had already been assembled should not be revisited again so that the risk of damaging the mirror reflector can be minimized. The last line of Eq. (7) denotes the constraint that all pieces should be properly assembled. Here a_1 and a_2 are the two positive defined constants, and L_l and L_r denote the total assembly path length of the left and right paths, which are given as

$$\begin{cases} L_l = \sum_{i=2}^{44} \|\mathbf{p}_{R2}[:, \mathbf{N}(i)] - \mathbf{p}_{R2}[:, \mathbf{N}(i-1)]\| \\ L_r = \sum_{i=2}^{49} \|\mathbf{p}_{R1}[:, \mathbf{M}(i)] - \mathbf{p}_{R1}[:, \mathbf{M}(i-1)]\| \end{cases}, \tag{8}$$

where the notation $\mathbf{B}(:, i)$ denotes the i'th column of matrix $\mathbf{B}$. The nonlinear optimization model defined in Eq. (7) can already be properly solved by existing solvers such as the GA, and since the symmetrical assembly path criterion is taken into consideration, only the optimization for R1 and R2 is required to accomplish the entire mission planning process. GA is a global nonlinear optimization algorithm, which simulates the evolution of the natural species, and the optimal solution to a problem is considered the final species that survives during natural competition. This algorithm has been implemented into many tool boxes such as MATLAB GA function and GA tool for C++. However, it has been proved that this optimization method has low efficiency[26] and will often converge to a local minimum solution. Therefore, improvements to the optimization model algorithms must be conducted.[27]

3 Modification of the Model and the Hybrid Optimization Method

In Sec. 2, it has been shown that the classic optimization process has certain drawbacks, so modifications and improvements have been made to increase the performance of the optimization algorithm. The discussion of this section is divided into two parts: the first section addresses the manipulator work space coverage effect, the maximum relative distance criterion, and the delay factor. The second section presents the hybrid optimization method for solving the assembly mission planning problem.

3.1 *Manipulator Work Space Coverage and Time-Delay Factor*

The work space of a manipulator is defined as the area that can be reached by the manipulator's end effector. When the manipulator base is deployed at a given position $\mathbf{r}$, the current reachable work space of the manipulator is defined as

$$W = [\mathbf{R} | \|\mathbf{R} - \mathbf{r}\| < L], \tag{9}$$

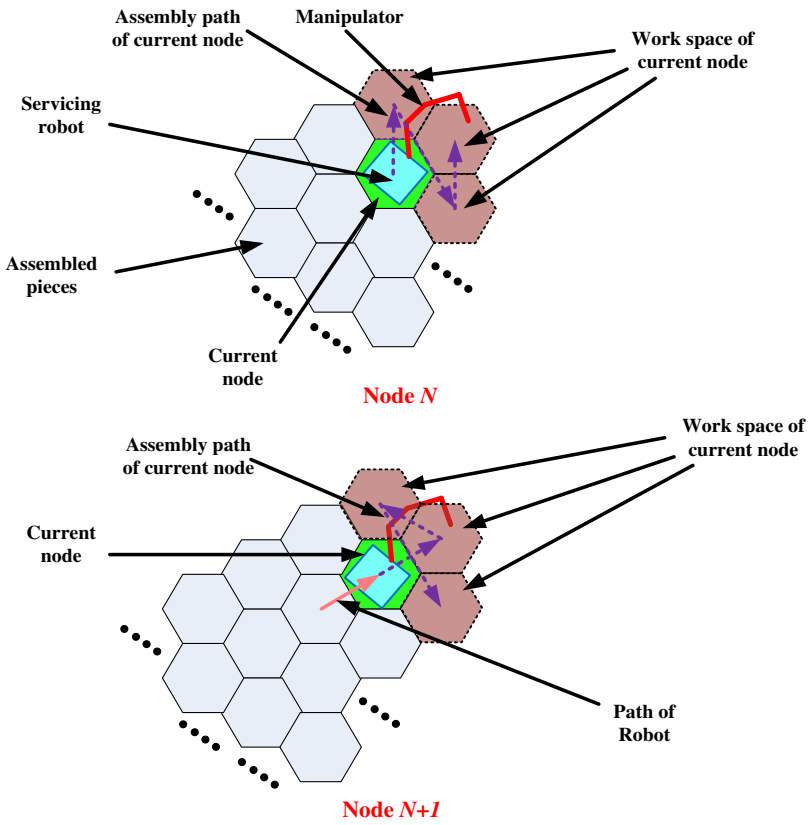

Fig. 4 Illustration of the manipulator work space coverage.

where L denotes the maximum reachable distance of the manipulator. Ideally, if a mirror segment is located within W, it should be installed by the end effector without moving the manipulator base. In this paper, it is assumed that the base is always connected to the telescope structure and that the assembly operation can only be carried out when the base is fixed to the telescope structure. Since the mass of the telescope is much larger than that of the manipulator, the coupling effect between the base and the manipulator can be ignored and the kinematic motion of the manipulator can be considered to be the same as the manipulators operating on ground. Therefore, the number of nodes of the assembly path can be further reduced since the base does not need to move to the location of each piece to realize the assembly operation. In this paper, the manipulator work space coverage is simplified using the connection matrix $\mathbf{\Theta}$. As shown in Fig. 4, the work space coverage of the manipulator is defined as

$$\begin{cases} \mathbf{r} = \mathbf{P}(i) \\ \mathbf{P}(j) \in W, \text{if } [\mathbf{\Theta}(i,j) = 1] \end{cases}. \tag{10}$$

From Eq. (10), it can be seen that if the manipulator base is located at $\mathbf{P}(i)$, the work space is defined as the pieces that are connected to $\mathbf{P}(i)$. This simplification can increase the calculation efficiency and make the optimization model much more realistic than the classic model. Figure 5 shows an example of the assembly path with manipulator work space coverage. It can be seen that the length of assembly path has been reduced. As the manipulator moves forward, the surrounding pieces are properly assembled, and the entire telescope reflector is properly covered.

The second modification of the optimization model is the maximum relative distance criterion, which is dedicated to finding the solution with the largest relative distance between manipulators. To install a piece, the manipulator collision-free trajectory must be generated by considering the motion constraint. If the relative distance between two manipulators is too small, the risk of collision becomes higher and more constraints must be considered. This effect may increase the burden of the manipulator motion planning and control system. Therefore, the new criterion is added into the system to obtain the assembly path with maximum relative

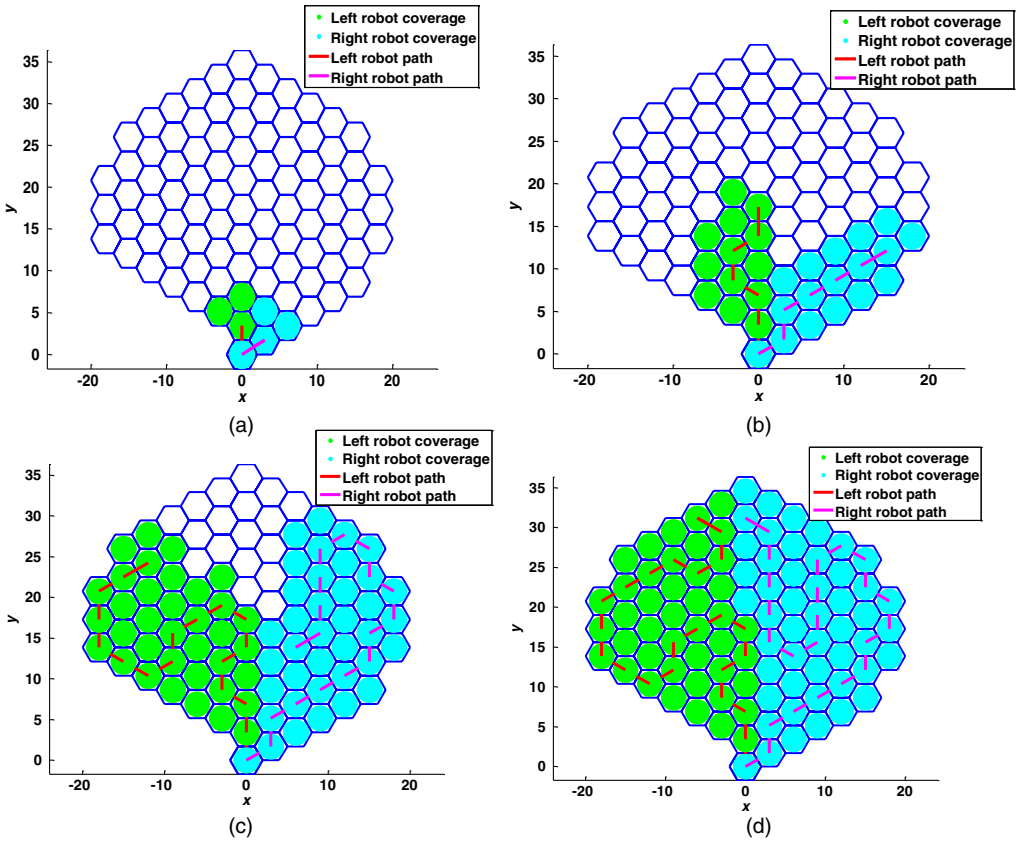

Fig. 5 Illustration of the manipulator work space coverage. (a) Step No. 2, (b) step Nos. 7 and 5, (c) step No. 20, and (d) final state.

distance between the robots. Since the work space coverage of the manipulator was defined in Eqs. (9) and (10), the max relative distance criterion is defined as

$$\max(\|\mathbf{r}_i - \mathbf{r}_j\| - 2 \cdot L), \quad \forall\ i \neq j, i, j = 1,2,3,..,6. \tag{11}$$

This modification can reduce the risk of accident during the in-orbit assembly process. Since the work space has been defined by the connection matrix in Eq. (10), the value of L is defined as $3/2\sqrt{3} \cdot l$, where l denotes the edge length of a hexagonal piece.

The third modification of the problem is focused on the time-delay factor. For the classic in-orbit assembly mission scenario, the manipulators are supposed to be functioning at exactly the same time step, and the delay problem has often been omitted. However, for the real space assembly missions, it may not be the case. First, the time needed for a manipulator to install a piece depends on many factors and may not be the same for each manipulator. Therefore, it is impossible for all manipulators to work at exactly the same pace. One solution to this problem is to set a predefined time interval for all manipulators, and the installation operation starts at the same time point. However, the choice of the time interval is difficult. If the interval is too large, the total assembly process may become less time-efficient. If the interval is too small, some of the manipulators may not be able to finish the installation operation in time and causes even more problems. Second, since the maximum distance criterion has been added into the system, it may be difficult for the algorithms to find a proper solution that satisfies all constraints. Therefore, the existence of the delay factor may increase the dimension of the candidate solution to the assembly path planning problem and ensures a better performance of the optimization algorithm. Based on the previous discussions, the modified optimization model is given as

$$\min_{\mathbf{N},\mathbf{M}}\left[a_1\cdot\sum_i L_l(i)+a_2\cdot\sum_i L_r(i)-g(\|\mathbf{r}_i-\mathbf{r}_j\|-2\cdot L)\right]$$
$$st.\begin{cases}\mathbf{N}=[\mathbf{N}1,\mathbf{N}2,\mathbf{N}3]\\ \mathbf{M}=[\mathbf{M}1,\mathbf{M}2,\mathbf{M}3]\\ \text{if } (N_i=N_j)||(M_i=M_j), j-i\le T_{\text{delay\_max}}\\ \max(\mathbf{N}i)\le 44\\ \max(\mathbf{M}i)\le 49\\ \mathbf{E}_i(t_f)=1,\ \forall\ i=1,2,3,\ldots,93\\ \mathbf{E}_i(t)=1,\text{if }[\mathbf{P}(i)\in W,\ \exists\ \mathbf{r}]\end{cases}. \tag{12}$$

By comparing Eq. (12) to Eq. (7), it can be seen that assembly sequence vectors $\mathbf{N}$ and $\mathbf{M}$ have been changed into three subvectors for the left path and the right path, respectively. This is due to the symmetrical assembly path criterion being removed so that the assembly path should be generated for all 6six robots. The cost function has also been modified since the path length is not the same for different robots. The third line of the constraint has also been changed. The constraints $N_i \neq N_j$ and $M_i \neq M_j$ have been removed due to the delay factor. A robot can now stay at a given position when other robots move to the next node. The positive constant $T_{\text{delay\_max}}$ denotes the maximum delay period that can be accepted. The existence matrix criterion has also been changed to include the work space coverage into the system. If a piece is within the work space of the manipulator, it is assumed that the piece can be properly assembled. Finally, $g(\|\mathbf{r}_i-\mathbf{r}_j\|\ge 2\cdot L)$ denotes the maximum relative distance criterion. In this paper, the cost function g is set to be the sum of the minimum relative distance between manipulators at each time step, which is noted as

$$g=\sum_n \min[\|\mathbf{r}_i(n)-\mathbf{r}_j(n)\|-2\cdot L],\quad \forall\ \mathbf{r}_i,\mathbf{r}_j\in\mathbf{P}(\mathbf{N}\cup\mathbf{M}). \tag{13}$$

Similar to Eq. (7), Eq. (12) can also be directly solved by existing optimizers. However, since the formulation of Eq. (12) is much more complex, the classic optimization solver will have very low efficiency and the calculation cost is too high to be handled by ordinary computers. Therefore, a new optimization algorithm is developed to ensure that the solver can be converged quickly to a local optimal solution, which has similar performance as the global optimizer.

3.2 *Hybrid Optimization Process*

In the previous section, three major modifications have been introduced into the optimization system. Consequently, the optimization model becomes much more complex, so it can no longer be efficiently solved by the classic global optimizers. To address this issue, a new optimization algorithm has been developed in this section. In Ref. 17, a continuous path generation algorithm (CPGA) has been presented based on the branch-and-bound method. The assumption has been made that the telescope reflector was planar and all hexagonal pieces have the same size so that the continuous path constraint is equivalent to the shortest assembly path. In this paper, this is not the case since the parabolic reflector is considered. However, a mapping can be obtained between the CPGA and the path with work space coverage. Assuming that the manipulator is located at position $\mathbf{r}$, the surrounding pieces are recognized by the CPGA and stored in matrix $\mathbf{F}$:

$$\mathbf{P}(i)\in\mathbf{F},\quad \text{if } [\mathbf{P}(i)\in W(\mathbf{r})]. \tag{14}$$

The CPGA will find the candidate propagation direction in $\mathbf{F}$ and finish the rest of the path generation operation. In this paper, the search for the candidate direction is modified to search for the local assembly path to install all of the elements within $\mathbf{F}$, and the manipulator work space coverage is generated as

$$\mathbf{E}_i(t) = 1, \quad \text{if } [\mathbf{P}(i) \in \mathbf{F}] \quad \text{and} \quad \mathbf{E}_i(t) = 0. \tag{15}$$

The algorithm stops when all of the pieces within the working region are installed by the corresponding manipulator. Therefore, by noting the local assembly path as

$$\mathbf{N}_{\text{local\_}n} = [\mathbf{N}_{\text{local\_}n}(1), \mathbf{N}_{\text{local\_}n}(2), .., \mathbf{N}_{\text{local\_}n}(i)], \quad i = \dim(\mathbf{F}), \tag{16}$$

the mapping can be found between the continuous path $\mathbf{N}_{\text{continuous}}$ and the path considering the work space coverage $\mathbf{N}_{\text{sc}}$:

$$\begin{cases} \mathbf{N}_{\text{continuous}} = [\mathbf{N}_{\text{local\_1}}, \mathbf{N}_{\text{local\_2}}, \ldots, \mathbf{N}_{\text{local\_}j}] \\ \mathbf{N}_{\text{sc}} = [\mathbf{N}_{\text{local\_1}}(\text{end}), \mathbf{N}_{\text{local\_2}}(\text{end}), \ldots, \mathbf{N}_{\text{local\_j}}(\text{end})] \end{cases}, \tag{17}$$

where the index j denotes the total node number of the continuous assembly path obtained by the CPGA. From Eq. (17), it can be seen that the mapping is injective, which implies that different CPGAs will generate different $\mathbf{N}_{\text{sc}}$. This effect is important for the optimization solver implementation since it proves that the optimization framework developed for CPGA can be directly adopted to solve the assembly path planning problem considering the manipulator work space coverage. Figure 6 demonstrates the effect of the mapping, where the CPGA result and the path with work space coverage are illustrated simultaneously. From the figure, it can be seen that the number of path nodes has been reduced and the path with work space coverage can be considered a subset of the group of continuous path solutions.

Once the assembly path with manipulator work space coverage is properly generated, the two-level hybrid optimization algorithm can be established. Based on the design of the optimization model, the optimization process is also separated into two phases. The first phase corresponds to the path optimization to find the minimum path length. The algorithm is based on the ant-colony-inspired algorithm, which has been proved to be efficient in finding the optimal trajectory of a complex system.[28] The second level of optimization is focused on the scheduling of the assembly sequence. The delay factor is considered and a working schedule with maximum inter-robotic distance is obtained. The flowchart of the optimization process is given in Fig. 7, where the two optimization levels are properly shown. It can be seen that the major difference between the hybrid optimization algorithm and the classic optimization algorithm lies in the aspect that the candidate path-generation process is replaced by the CPGA, which is much more efficient. According to Eqs. (7) and (12), it can be seen that the assembly path is considered a constraint in the optimization model. To address this issue, finding a feasible solution that satisfies all of the path constraints can take a huge amount of time. However, using the mathematical mapping obtained in Eq. (17) can significantly increase the calculation efficiency, which proves the advantage of the method proposed in this paper.

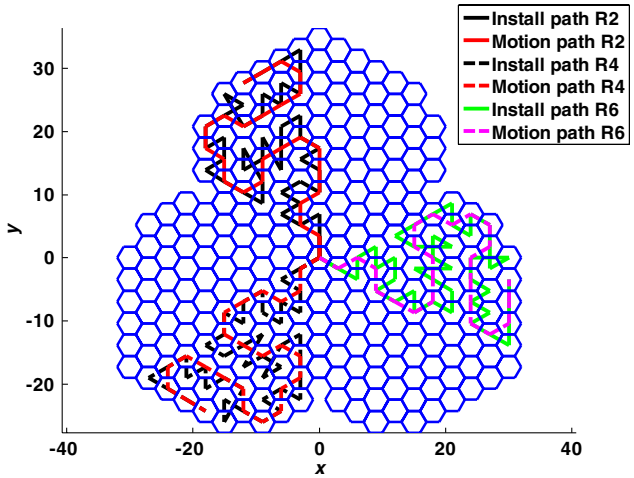

Fig. 6 The mapping between the continuous path and the work space coverage path.

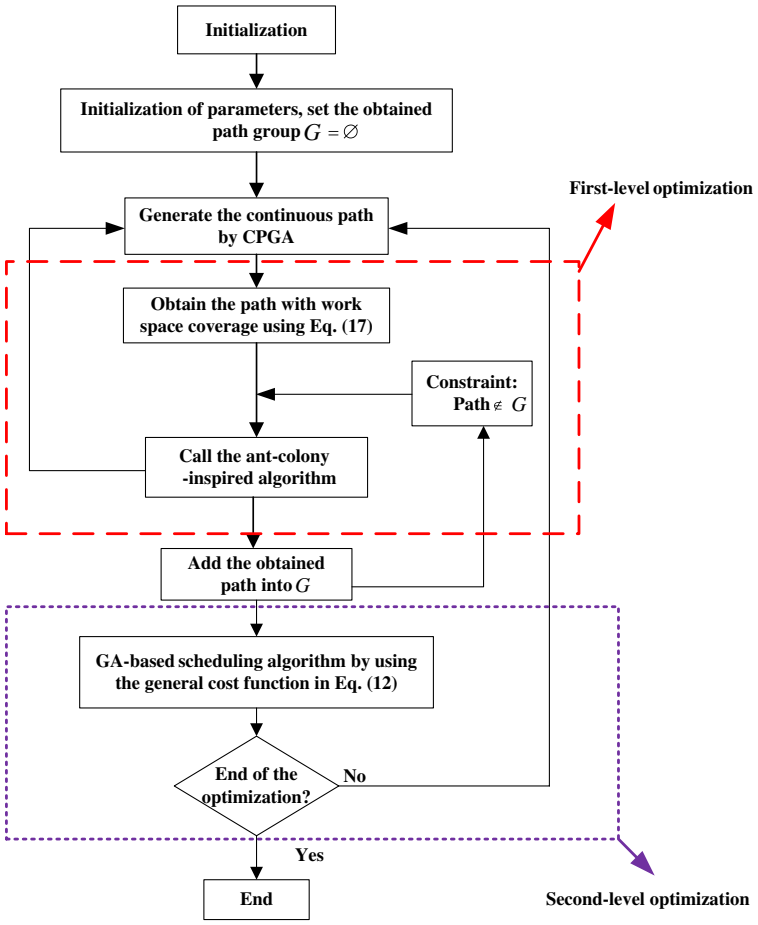

Fig. 7 Demonstration of the two-level optimization algorithm.

By analyzing Eq. (12), it can be seen that the mission planning and scheduling operations are considered separately. The first part of the cost function is directly linked to the mission planning aspect, which corresponds to the generation of the assembly path. The second part of the cost function is dedicated to obtaining an appropriate working schedule with a given path. Therefore, the mission scheduling process can be considered a second optimization phase that takes the result of first optimization phase as input.

4 Simulation and Analysis

This section demonstrates the simulation results of the algorithms proposed in this paper. Since the optimization algorithm is divided into two levels, the discussion in this section is also conducted in two parts, which corresponds to the mission planning and scheduling process, respectively.

4.1 *Test of the Mission Planning Algorithm*

The first part of the simulation test is dedicated to test the assembly path planning method. As cited previously, the general optimization models described in Eqs. (7) and (12) can both be handled by MATLAB GA solvers. Thus, the comparison is made between GA and the proposed algorithms. The basic system parameters are shown in Table 1.

The demonstration of the simulation results is done in three parts. First, the symmetrical assembly path criterion is taken into consideration, and Fig. 8 shows the comparison of the total path length obtained by different algorithms. The red dot lines denote the results obtained by

Table 1 System parameters.

Dynamic parameters	Value
Hexagonal piece length	2 m
Total piece number	274
Maximum path node number N	49
Telescope aperture	60 m
Number of working regions	6
Starting point of assembly process	[0,0,0]
T_{delay_max}	10 H
Left/right path node number	44, 49

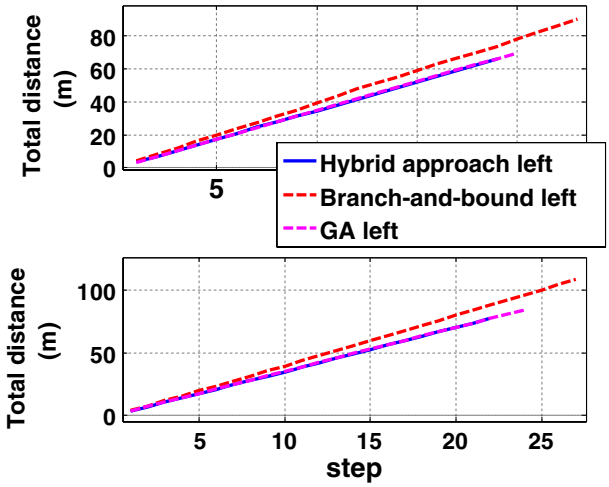

Fig. 8 Comparison of total path length obtained by different solvers.

considering the antenna surface to be planar.[17] The pink dot lines denote the GA results of Eq. (7), and the blue lines represent the optimization results obtained by the two-level algorithm developed in this paper. From the comparison, it can be seen that the planar antenna model can no longer obtain the optimal solution, while the results obtained by GA solver and the hybrid algorithm have good agreement. It can also be seen that the hybrid algorithm's performance is slightly better than the GA solver. This may be due to the high calculation cost and complex model leading the GA solver to converge to a local minimum solution.

Second, the optimization models presented in Eq. (7) and (12) are compared to illustrate the effect of the maximum inter-robotic distance criterion. The simulations are shown in Figs. 9–14. Figure 9 shows the accumulation of the minimum relative distance and the sum of all relative distances between robots at each assembly step. Figure 10 shows the variation of minimum inter-robotic distance as a function of assembly step. From the results, it can be seen that the relative distance between robots is slightly increased by the maximum relative distance criterion, but the improvement is not significant.

To improve the performance of the maximum relative distance criterion, the unsymmetrical assembly path is taken into consideration. Figures 11 and 12 show the comparison of relative distance variation between the robots during the mission assembly process. It can be seen that since the unsymmetrical assembly path criterion increases the dimension of candidate solution group, the relative distance between manipulators are further increased. Figures 13 and 14 depict

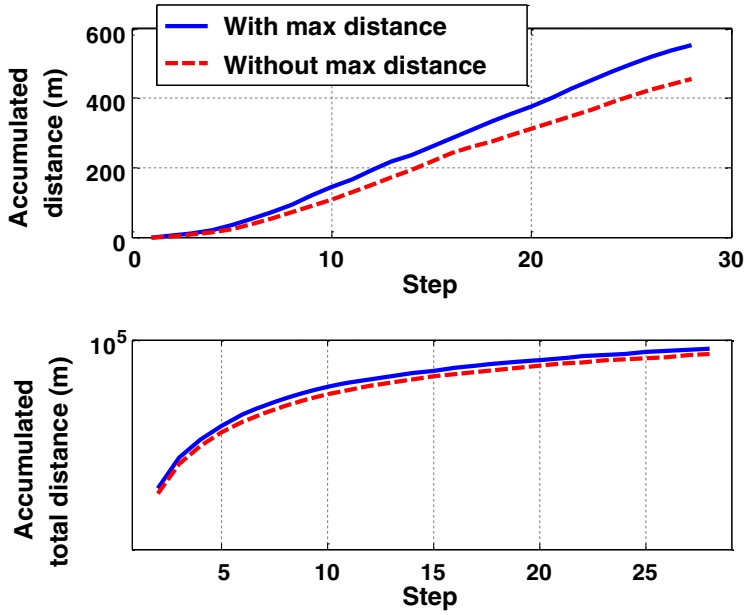

Fig. 9 Comparison of the minimum distance between the robots and the accumulated distance.

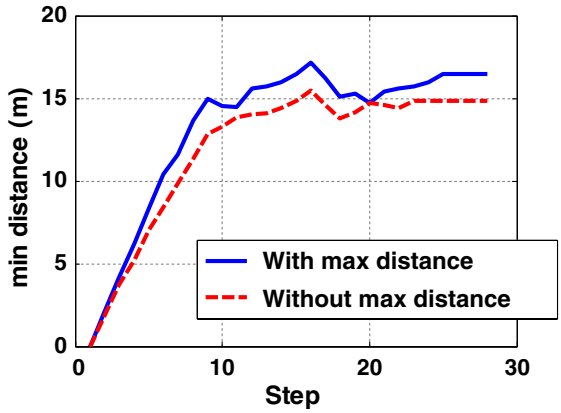

Fig. 10 Comparison of the relative minimum distance obtained at each time step.

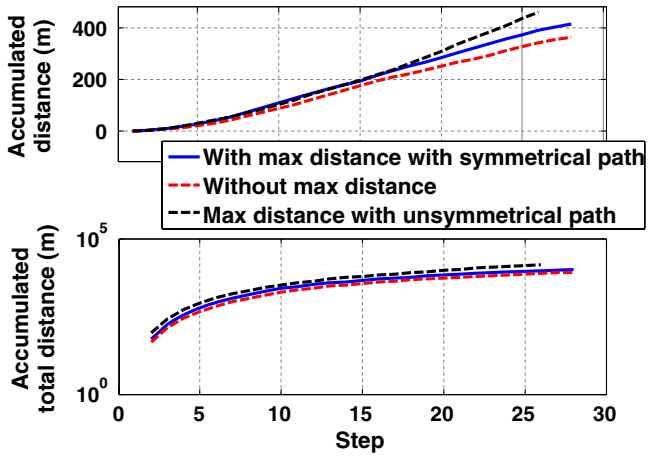

Fig. 11 Comparison of the minimum distance between the robots and the accumulated distance.

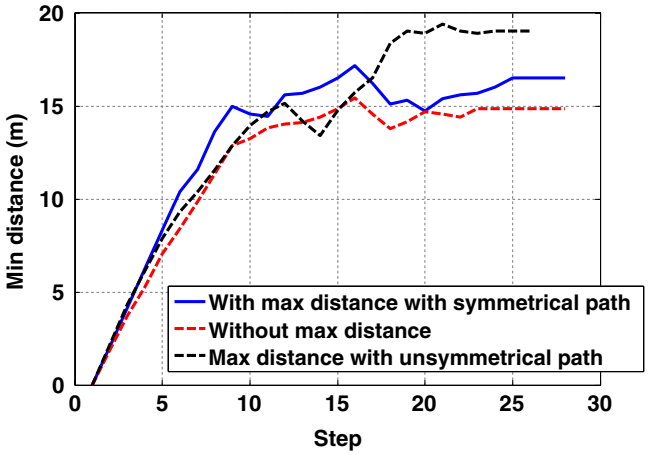

Fig. 12 Comparison of the relative minimum distance obtained at each time step.

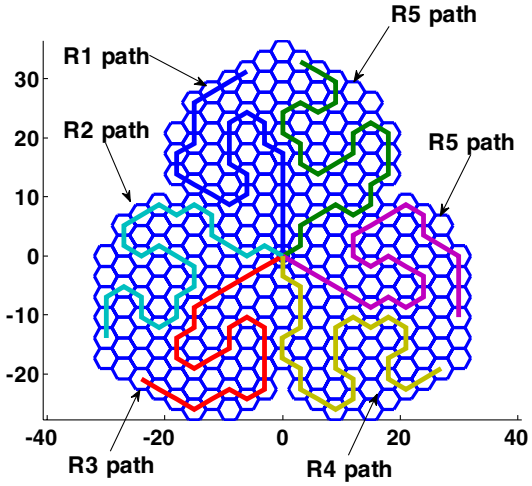

Fig. 13 Illustration of the optimization result with symmetrical path condition.

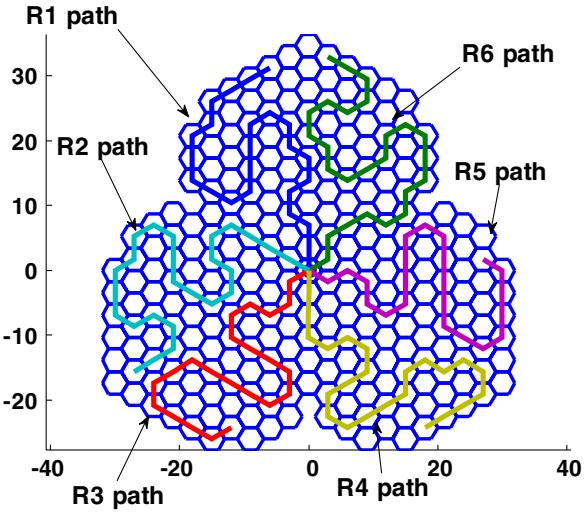

Fig. 14 Illustration of the optimization result without symmetrical path condition.

the configuration of the symmetrical and unsymmetrical assembly paths, where the working regions for different manipulators can be properly recognized.

4.2 *Test of the Mission Scheduling Algorithm*

This section is dedicated to illustrating the effectiveness of the mission scheduling algorithm developed in this paper. According to the discussion in the previous section, since no delay factor has been considered, the optimization algorithm can only improve the relative distance with limited performance. To address this issue, the mission scheduling algorithm is adopted and the relative distance between robots are obtained and shown in Fig. 15. Similarly, the accumulation of relative distance throughout the in-orbit assembly process is shown in Fig. 16. From these figures, it can be seen that the average relative distance and the accumulated relative distance are dramatically increased by the time-delay factor. By adding the delay factor, the algorithm seeks to stop the manipulator's motion if the relative distance becomes smaller than a predefined threshold. At the same time, an adaptive law has also been implemented into the algorithm to prevent the case in which all of the robots are blocked by the delay factor. When all robots are blocked, the minimum distance threshold is adjusted to be smaller so that at least one robot can keep moving. With this design, the accomplishment of the assembly mission can be guaranteed while maximizing the average relative distance between manipulators.

As discussed previously, the relative distance between manipulators can be properly increased by including the time-delay factor in the optimization process, which can dramatically

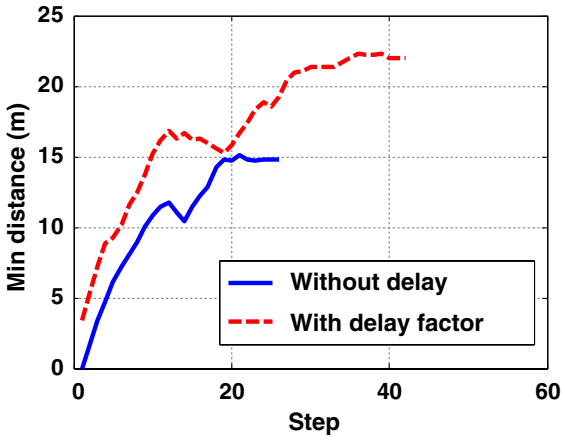

Fig. 15 Comparison of the relative minimum distance obtained at each time step.

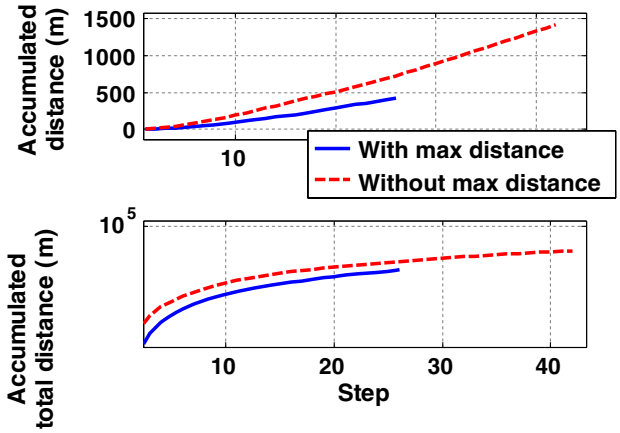

Fig. 16 Comparison of the minimum distance between the robots and the accumulated distance.

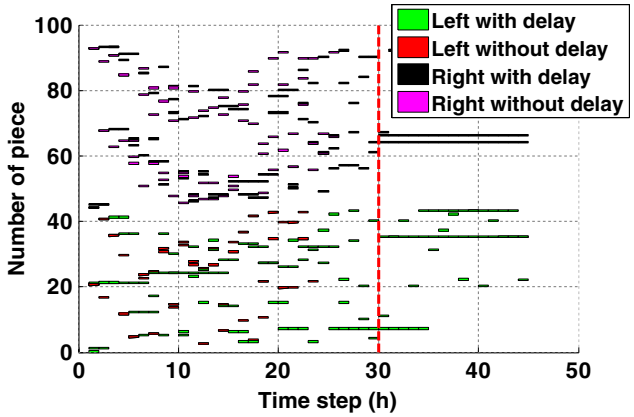

Fig. 17 Comparison of the assembly schedules obtained by different approaches.

simplify the manipulator path planning and control process and reduce the risk of accidents such as collision or damage to the mirror structure. However, the cost of this improvement is increasing the total assembly period. The mission assembly schedule is shown in Fig. 17 to better analyze the result. From the figure, it can be seen that the entire assembly process can be accomplished within 30 h without the time-delay factor, while it takes more than 40 h to realize the assembly with the delay of the manipulator. Finally, Fig. 18 shows the mission scenario of the assembly process, considering all factors mentioned in this paper. It can be seen that the work space coverage of the manipulator and the unsymmetrical assembly path are properly adopted,

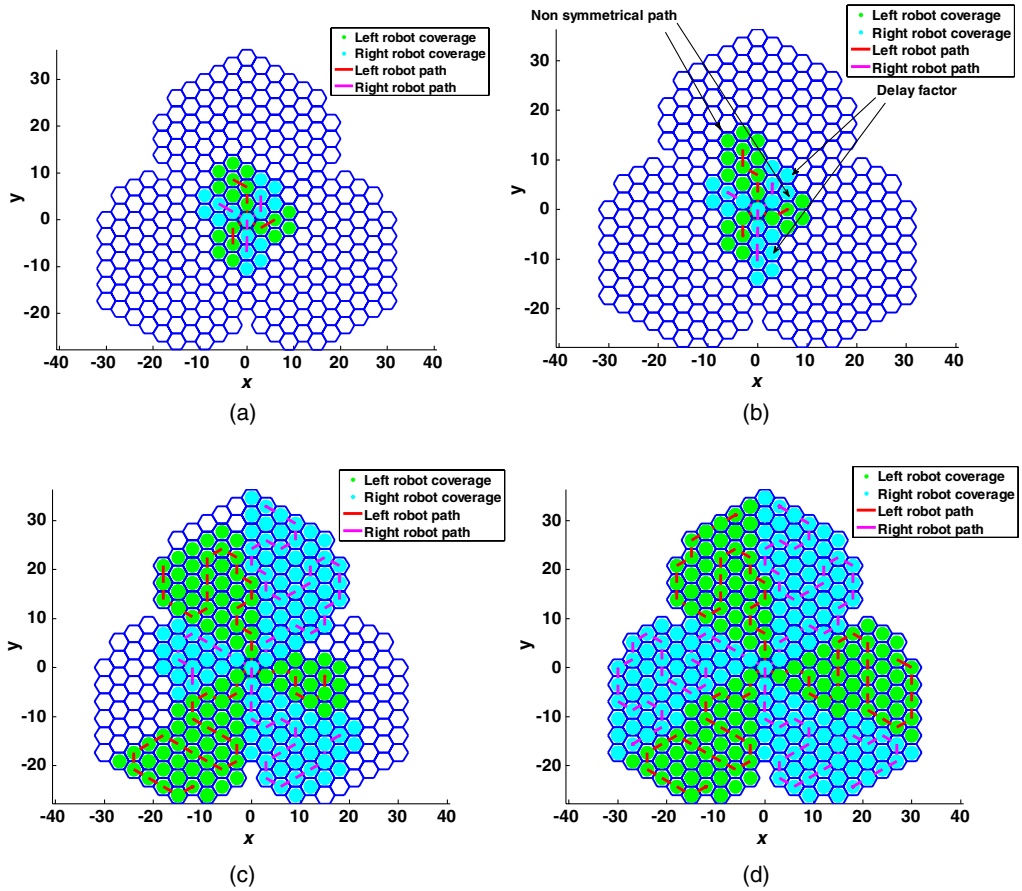

Fig. 18 Illustration of the assembly process considering all constraints and criteria. (a) Effect of unsymmetrical path, (b) effect of delay factor, (c) R3 and R6 completed, and (d) final state.

and the delay factor has an important impact on the assembly process. In Fig. 18(c), it can be seen that the assembly task of R3 and R6 have already been accomplished, while R5 has finished less than 50% of the total work.

5 Conclusion

This paper investigates the LST mirror reflector in-orbit assembly problem. A detailed mission scenario has been designed by considering the 3-D parabolic reflector surface, the task assignment of multirobots, the manipulator work space coverage, and the time-delay factors. To properly solve the complex optimization model, a new algorithm that establishes a fast candidate path generation has been proposed. A two-level hybrid optimization framework has also been developed to solve the mission planning and scheduling problems separately. Based on the simulation results, the conclusions show that the new mission design is more efficient and can better represent the real mission environment. The proposed algorithm can effectively solve the complex mission optimization problem and lead the solver to converge rapidly to a result that is close to the global optimal solution. Therefore, this paper provides a new potential option for future LST design and mission analysis. Meanwhile, it should be pointed out that this paper assumes that the robots have already loaded all of the pieces at the beginning of simulation. However, in the real mission scenario, this may be difficult to realize. To address this issue, the robot might need to come back to the initial point to reload the pieces, and this effect may impact the mission planning process. This is an important factor, and the related results will be the focus in our future works.

Acknowledgments

This work was partially supported by the National Natural Science Foundation of China (Grant Nos. 11972182 and U1637207), sponsored by Qing Lan Project, funded by Science and Technology on Space Intelligent Control Laboratory (Grant No. HTKJ2019KL502012), and Funding for Outstanding Doctoral Dissertation in NUAA (Grant No. BCXJ18-02). The authors fully appreciate their financial support.

References

1. N. Lee et al., "Architecture for in-space robotic assembly of a modular space telescope," *J. Astron. Telesc. Instrum. Syst.* **2**(4), 041207 (2016).
2. J. Nella et al., "James Webb Space Telescope (JWST) observatory architecture and performance," *Proc. SPIE* **5487**, 576–587 (2004).
3. W. Oegerle et al., "Concept for a large scalable space telescope: in-space assembly," *Proc. SPIE* **6265**, 62652C (2006).
4. Z. Cheng et al., "In-orbit assembly mission for the Space Solar Power Station," *Acta Astronaut.* **129**(3), 299–308 (2016).
5. R. Li, S. Wang, and M. Wu, "Numerical simulation of closest vane thermal performance in large aperture space solar telescope," *Appl. Therm. Eng.* **103**(25), 952–960 (2016).
6. C. D. Lillie, R. Dailey, and S. Polidan, "Large aperture telescopes for launch with the Ares V launch vehicle," *Acta Astronaut.* **66**(3), 374–381 (2010).
7. X. Pan and M. Xu, "Distributed situational observer in a displaced orbit: relative dynamics and control," *J. Astron. Telesc. Instrum. Syst.* **4**(4), 045001 (2018).
8. S. Mohan and D. W. Miller, "Dynamic control model calculation: a model generation architecture for autonomous on-orbit assembly," *J. Spacecr. Rocket* **51**(5), 1430–1453 (2014).
9. L. Shi, N. Kinkaid, and J. Katupitiya, "Robust control for satellite attitude regulation during on-orbit assembly," *IEEE Trans. Aerosp. Electron. Syst.* **52**(1), 49–59 (2016).
10. S. Bandyopadhyay and S. Chung, "Nonlinear attitude control of spacecraft with a large captured object," *J. Guidance, Control Dyn.* **39**(4), 754–769 (2016).

11. P. Gasbarri, R. Monti, and M. Sabatini, "Very large space structures: non-linear control and robustness to structural uncertainties," *Acta Astronaut.* **93**(2) 252–265 (2014).
12. H. Siguerdidjane and Y. Somov, "Nonius guidance and robust image motion stabilization of a large space astronomical telescope," *IFAC Proc. Vol.* **44**(1), 5142–5147 (2011).
13. Y. She and S. Li, "Optimal slew path planning for the Sino-French space-based multiband astronomical variable objects monitor mission," *J. Astron. Telesc. Instrum. Syst.* **4**(1), 017001 (2018).
14. J. Lymer et al., "Commercial application of in-space assembly," in *AIAA SPACE Forum*, Long Beach, California, AIAA 2016–5236 (2016).
15. X. Wang, S. Li, and Y. She, "Concept design and cluster control of advanced space connectable intelligent microsatellite," *Acta Astronaut.* **141**(2), 1–7 (2017).
16. S. Yano et al., "Improvements in and actual performance of the plant experiment unit onboard Kibo, the Japanese experiment module on the International Space Station," *Adv. Space Res.* **51**(5), 780–788 (2013).
17. Y. She et al., "On-orbit assembly mission planning considering topological constraint and attitude disturbance," *Acta Astronaut.* **152**(11), 692–704 (2018).
18. A. Stolfi, P. Gasbarri, and M. Sabatini, "A parametric analysis of a controlled deployable space manipulator for capturing a non-cooperative flexible satellite," *Acta Astronaut.* **148**(2), 317–326 (2018).
19. C. Saunders et al., "Building large telescopes in orbit using small satellites," *Acta Astronaut.* **141**(4), 183–195 (2017).
20. C. Underwood et al., "Using CubeSat/micro-satellite technology to demonstrate the Autonomous Assembly of a Reconfigurable Space Telescope (AAReST)," *Acta Astronaut.* **114**(2), 112–122 (2015).
21. A. Badawy and C. McInnes, "On-orbit assembly using superquadric potential fields," *J. Guidance Control Dyn.* **31**(1), 30–43 (2008).
22. R. Foust, S. Chung, and F. Hadaegh, "Autonomous in-orbit satellite assembly from a modular heterogeneous swarm using sequential convex programming," in *AIAA/AAS Astrodyn. Spec. Conf.*, AIAA 2016–5271 (2016).
23. D. Izzo, L. Pettazzi, and M. Ayre, "Mission concept for autonomous on orbit assembly of a large reflector in space," in *56th Int. Astronaut. Congr.*, Paper IAC-05-D1.4.03 (2005).
24. T. Chen et al., "Output consensus and collision avoidance of a team of flexible spacecraft for on-orbit autonomous assembly," *Acta Astronaut.* **121**(3), 271–281 (2016).
25. T. Chen and H. Wen, "Autonomous assembly with collision avoidance of a fleet of flexible spacecraft based on disturbance observer," *Acta Astronaut.* **147**(4), 86–96 (2018).
26. Y. She, S. Li, and Y. Zhao, "Onboard mission planning for agile satellite using modified mixed-integer linear programming," *Aerosp. Sci. Technol.* **72**(2), 204–216 (2018).
27. V. A. Eremeev and Y. V. Kovalenko, "Genetic algorithm with optimal recombination for the asymmetric travelling salesman problem," in *Int. Conf. Large-Scale Sci. Comput.*, pp. 341–349 (2017).
28. M. Ceriotti and M. Vasile, "MGA trajectory planning with an ACO-inspired algorithm," *Acta Astronaut.* **67**(10), 1202–1217 (2010).

Yuchen She is currently a fourth-year PhD student at the School of Astronautics, Nanjing University of Aeronautics and Astronautics. He received his bachelor's degree in physics from the University of Toulouse and his master's degree in aerospace technology from the Institute of Astrophysics and Planetology, Toulouse, France. His major research interest is space robotics and spacecraft dynamics and control.

Shuang Li received his BSE and MSE degrees, and his PhD from the Department of Aerospace Engineering at Harbin Institute of Technology, China, in 2001, 2003, and 2007, respectively. Since 2007, he has been with the College of Astronautics, Nanjing University of Aeronautics and Astronautics, China, where he is a full professor. He was also a visiting scholar of the Department of Mechanical and Aerospace Engineering at the University of Strathclyde from 2012 to 2013. He has authored over 80 articles in reputable journals and conference proceedings. His research interests include spacecraft dynamics and control, deep space exploration, spacecraft autonomous guidance navigation and control, and astrodynamics. He has undertaken and

is conducting up to 20 projects sponsored by the China government and the aerospace enterprises in these fields.

Yufei Liu received his PhD in spacecraft design from Harbin Institute of Technology, China, in 2007. Since then, he has been an engineer at the China Academy of Space Technology. Currently, he is a senior engineer at Duan baoyan Academician workstation in Qian Xuesen Laboratory of Space Technology. His research interests include deep space exploration mission design, autonomous navigation, dynamics and control of large space structures, solar sail, and space solar power station.

Menglong Cao received his BS degree in manufacturing process automation and his MS degree in control theory and control engineering from the Qingdao University of Science and Technology, China, in 1996 and 2005, respectively, and his PhD in navigation, guidance, and control from the Harbin Institute of Technology, China, and in 2009. From 2010 to 2012, he held a postdoctoral researcher in control theory and control engineering with Northeastern University, China. Currently, he is an associate professor with the College of Automation and Electronic Engineering, Qingdao University of Science and Technology. His current research interests include automatic navigation, intelligent control, and information fusion.